Meteorologische Zeitschrift, Vol. **25**, No. 1, 37–53 (published online June 17, 2015)

ICAM 2013

Impact of Radar Data Assimilation on the Numerical Simulation of a Severe Storm in Croatia

Antonio Stanesic[1]* and Keith A. Brewster[2]

[1]Meteorological and Hydrological Service (DHMZ) of Croatia, Zagreb, Croatia
[2]Center for Analysis and Prediction of Storms, University of Oklahoma, Norman, OK USA

(Manuscript received December 31, 2013; in revised form January 15, 2015; accepted January 25, 2015)

Abstract

A severe thunderstorm hit the northwestern part of Croatia in the late afternoon and evening of 24 June 2008. This severe event is used as a test case for the Advanced Regional Prediction System (ARPS) high resolution numerical prediction model and for exploring the impact of assimilating conventional and radar data. Radar radial velocity data were assimilated using three-dimensional variational analysis (3DVAR). Radar reflectivity data were used through a cloud analysis procedure where hydrometeors and cloud fields are defined, and adjustments to the in-cloud temperature and moisture fields are made. Results show that without data assimilation, the models were not able to represent the development of the storm nor the proper environment for it. Assimilation of surface observations in the mesoscale outer model provided spatial distribution of convection ingredients that established a proper environment for storm initiation and propagation. Without that, the inner storm-scale model, even with radar data assimilation, is unable to simulate storm development. Using the outer model with assimilation of surface data in combination with an inner model including assimilation of radar data provided the best simulation of storm initiation and development.

Keywords: radar data assimilation, severe storm, numerical weather prediction, ARPS

1 Introduction

Severe thunderstorms are among the most hazardous weather phenomena in many European countries. These storms can produce strong wind gusts, tornado, hail and heavily rainfall; thus they possess a great threat to human lives and to material goods. Dotzek et al. (2009) reported an estimated cost of 5–8 billion EUR annually from severe thunderstorms in Europe. In Croatia, such events are common during the summer months in the central and northern parts of Croatia. As these are mostly agricultural regions, they result in heavy damage to agricultural production.

Romero et al. (2007) provided European climatology for some severe convective storm environmental variables using ERA40 (European Centre for Medium-Range Weather Forecasts (ECMWF) re-analysis of the global atmosphere and surface conditions for 45-years, over the period from September 1957 through August 2002 by ECMWF; Uppala et al., 2005). They showed that an environment favorable for severe thunderstorm development in Europe is commonly found along a latitudinal belt over south-central Europe. Both thermodynamic and dynamic ingredients for severe-storm development are present in the climatology. Favorable thermodynamic conditions are most prevalent in the south due to the influence of the warm waters of southern Adriatic and Mediterranean while dynamic forcing is most common along well-defined Atlantic and Western Europe cyclone tracks. Similarly, Brooks et al. (2003) used "pseudo-soundings" from the reanalysis system (National Centers for Environmental Prediction (NCEP) and National Center for Atmospheric Research (NCAR) high-resolution global analyses of atmospheric fields from January 1948 through July 2002; Kalnay et al., 1996) to find environmental conditions associated with significant severe thunderstorms and to make global estimate of the frequency of their occurrence. They reported that the greatest frequency of conditions favorable for severe thunderstorm development in Europe is found over the Spanish plateau and the region east of the Adriatic Sea, including Croatia.

Favorable conditions for severe thunderstorms are most commonly found in the northern part of Croatia, located in the southern and southwestern Pannonian basin; severe thunderstorms are common in Croatia during summer months. Pannonian basin is located at southeastern part of Central Europe. It is surrounded by the Carpathian Mountains, the Alps, the Dinarides and the Balkan mountains (Fig. 1). The northern part of Croatia is located within the south and southwestern portion of Pannonian basin, with some smaller mountains in northwestern Croatia. Typical meteorological situations in which thunderstorms occur in the Pannonian basin include warm season frontal passage, waves of frontal systems, cutoff cyclones, or upper-level cold pools with positive vorticity maxima (Horváth and Geresdi, 2001; Horváth and Geresdi, 2003). Horvath et al. (2008) also identified Type B-II cyclones as

*Corresponding author: Antonio Stanesic, Meteorological and Hydrological Service (DHMZ) of Croatia, Gric 3, 10000 Zagreb, Croatia, e-mail: antonio.stanesic@cirus.dhz.hr

DOI 10.1127/metz/2015/0574

Gebrüder Borntraeger Science Publishers, Stuttgart, www.borntraeger-cramer.com

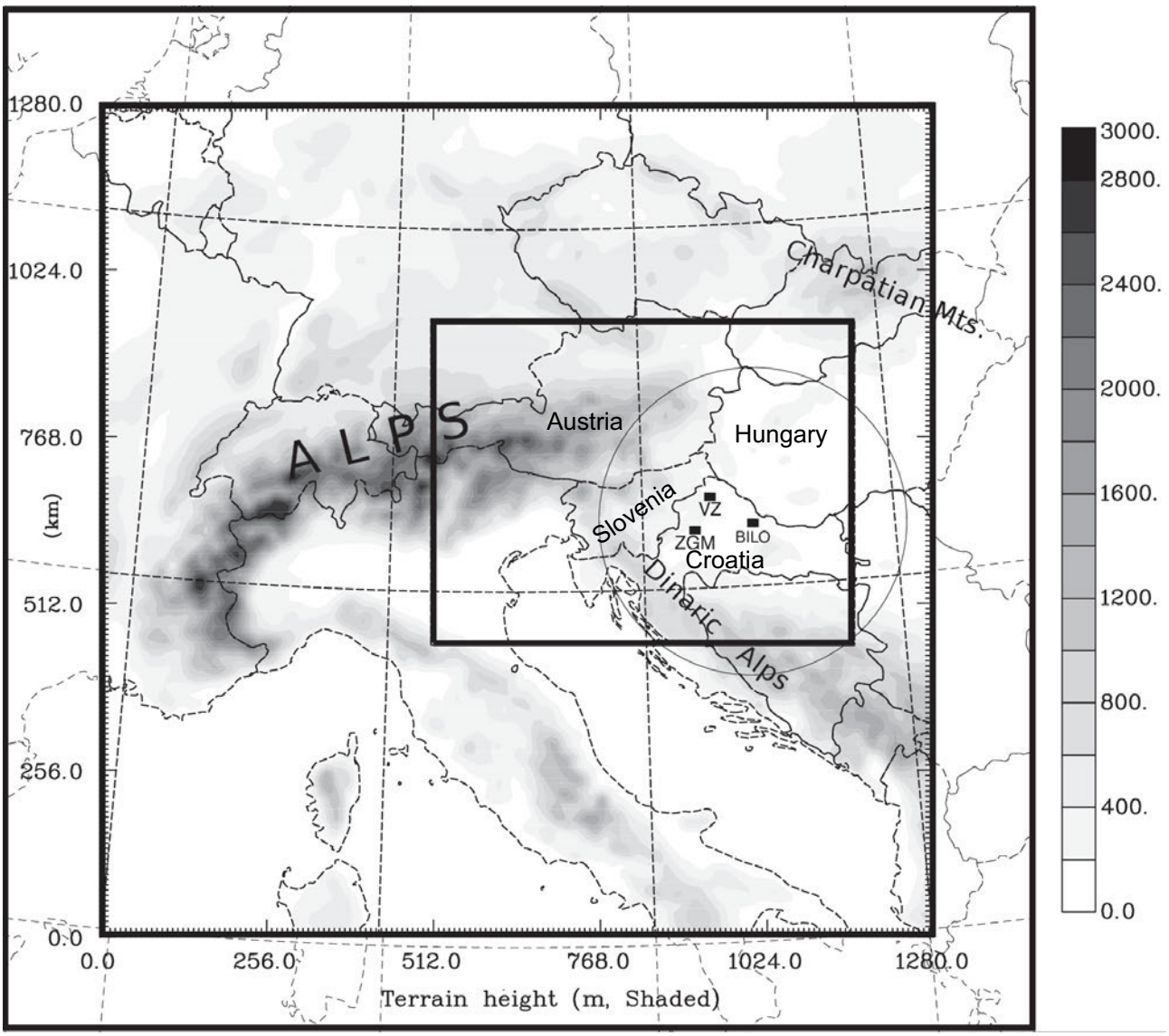

Figure 1: Domains of three ARPS configurations: ARPS24 (horizontal grid spacing 24 km) – biggest rectangle, ARPS8 (horizontal grid spacing 8 km) – middle rectangle and and ARPS2.5 (horizontal grid spacing 2.5 km) smallest rectangle. Shading represents terrain height in ARPS8 configuration. Also shown are location of Zagreb Maksimir sounding (ZGM), town Varazdin (VZ) and Bilogora radar (BILO). Thin circle around Bilogora radar represents maximum range of Bilogora radar (240 km). Name of countries and surrounding mountain ranges are indicated.

source of high impact weather during summer. Type B-II cyclones are initiated in the western part of the central Adriatic; they have weak intensity and small scale, and they were the least predictable of all cyclone types identified in their study.

In many countries of Europe an ingredient based approach is used for forecasting of such severe storm events, yet the forecasting is difficult. One significant challenge is that small horizontal grid spacing must be used in order to represent small-scale convective processes in numerical models, requiring significant computing resources. Still, a number of experiments have been done with research models in order to gauge their ability to simulate convective storms in Europe (e.g., Ducrocq et al., 2002; García-Ortega et al., 2007; Nuissier et al., 2008; Cohuet et al., 2011; Mastrangelo et al., 2011).

Severe convective storms in the Pannonian Basin are not often investigated. Studies done for storms in the Pannonian Basin include Strelec et al. (2007) who performed numerical simulation of two thunderstorms (squall line and super-cell) with the NCAR-PSU Mesoscale Model-5 (MM5, Grell et al., 1994). The horizontal grid spacing used was 3 km and during the first two hours of simulation surface observations were introduced via analysis nudging. The model simulated the squall line development quite well, but there was a notable shift in time compared to the actual development. Similar results were obtained for the supercell simulation, where forecasted storm development was late by at least 1 h compared to the actual development. Horváth et al. (2007) performed numerical simulation of a severe storm that hit Budapest on August 20, 2006. The model used was the MM5 Version 3 with horizontal

grid spacing of 1.5 km. Several experiments were performed while varying the initial time; the initial conditions for all were obtained by interpolating global model fields. In one of the experiments local radar data were assimilated. All simulations correctly predicted cold front passage over Budapest, but only the simulation using radar data assimilation predicted the storm development as observed. Benefits of radar data assimilation were also found in previous studies where it was shown that initialization of convective-scale numerical models with high resolution radar data is beneficial for forecasting convective storm development and for improving precipitation forecast (e.g. Sun J., 2005; Seity et al., 2011). Additionally, using three-dimensional variational data assimilation (3DVAR) to assimilate radar radial velocity (Xiao et al., 2005) or both, radar radial velocity and reflectivity (Xiao and Sun, 2007) in high resolution numerical model has led to improvement of skill for short-range heavy rainfall forecast. Souto et al. (2003) used radar reflectivity data to initialize moisture variables in high resolution numerical model via cloud analysis procedure and found that it improves precipitation pattern and amount.

The main goal of this study is to assess sensitivity of numerical simulation of a severe convective storm in the Pannonian Basin with a cloud-scale numerical model to (1) horizontal grid spacing, (2) assimilation of conventional observations (SYNOP) and/or (3) assimilation of high resolution observations (radar observation).

In Section 2 methods used in this research are presented while in Section 3 an overview of the case, including the synoptic situation and analysis of the storm using radar observations is given. Results from numerical simulation experiments are presented in Section 4, and summary and conclusions are given in Section 5.

2 Methods

2.1 Observations

Two types of observations were used in this study. First are surface synoptic stations (SYNOP) data from the European network of manned or automated weather stations. And second are raw radar data from Croatia radar. Hourly Europe SYNOP data were obtained for the period 1500–1800 UTC 24 June 2008, and temperature, pressure, horizontal wind components and relative humidity were used in the assimilation procedure.

The radar data used in this study comes from the Bilogora radar located in northern Croatia (lat = 45 ° 53 ′ N, lon = 17 ° 12 ′; Fig. 1). The Bilogora radar is a Doppler S-band (10-cm) radar (DWSR 88 S), with a nominal maximum range of 240 km, 2 ° beam width and volume scans every 15 minutes at 15 elevations from 0 to 34.9°. The Bilogora radar is also used in directing hail suppression activities, and while hail suppression is active it uses fewer elevations for scanning and provides a reduced number of products. Data available for this case are full volume scans every 15 minutes from 1500–2100 UTC, with data after 1915 being reduced due to hail suppression activities.

Before assimilation of radar data two additional steps were performed on raw radar data. In the first step data were quality-controlled which included: removal of anomalous propagation artifacts, removal of transient echoes in clear sky and radial velocity unfolding. The second step involved remapping of radar data from polar coordinates to the Cartesian terrain-following model grid (2.5 km horizontal grid spacing). Remapping uses a least-square fit to local polynomial function that is quadratic in the horizontal and linear in the vertical and it has properties of smoothing radar data near radar site and it acts as interpolator at longer ranges from radar. Thus no additional superobbing neither radar data thinning was applied on remapped data. More on radar data preprocessing in framework of ARPS model can be found in Brewster et al. (2005). Quality of radar data preprocessing can be assessed on Fig. 2 where original and remapped radar data is shown. At lowest PPI scan of radar radial velocity aliasing in original data is evident where high values are present (Nyquist velocity: 16.5 m/s). On the other hand radar preprocessing removes aliased data and replaces it with corrected values and fills some gaps where data in radar image was not present. Similar and more pronounced filling and dealiasing of radar radial velocity data was performed in vertical cross section. Vertical cross section of radar reflectivity shows that in remapped data most of observed structures are preserved except those of very small spatial scale (BWER is not resolved in remapped data).

2.2 Modeling methodology

This study used the Advanced Regional Prediction System (ARPS) high resolution non-hydrostatic numerical prediction model, version 5.2 (Xue et al. 1995, 2000, 2001). ARPS is a three-dimensional, nonhydrostatic model in generalized terrain-following coordinates with equal-spacing in the horizontal and user-specified stretching in the vertical. It was designed for numerical simulation of storm-scale phenomena, so in addition to appropriate physics and dynamics it incorporates tools and methods for ingesting observational data, both conventional and observations of high temporal and spatial density (e.g. radar data). In this study ARPS was used with a few one-way nested grids with model horizontal grid spacing of 24 km (ARPS24), 8 km (ARPS8) and 2.5 km (ARPS2.5). The domains of all ARPS configurations are shown on Fig. 1. In the vertical dimension, 58 levels were used with average vertical grid spacing of 350 m and minimum grid spacing of 40 m, which places the first scalar grid level at 20 m above ground level (AGL). Initial and lateral boundary conditions (3 hourly) for the coarsest ARPS (ARPS24) grid were obtained from Global Forecast System (GFS)

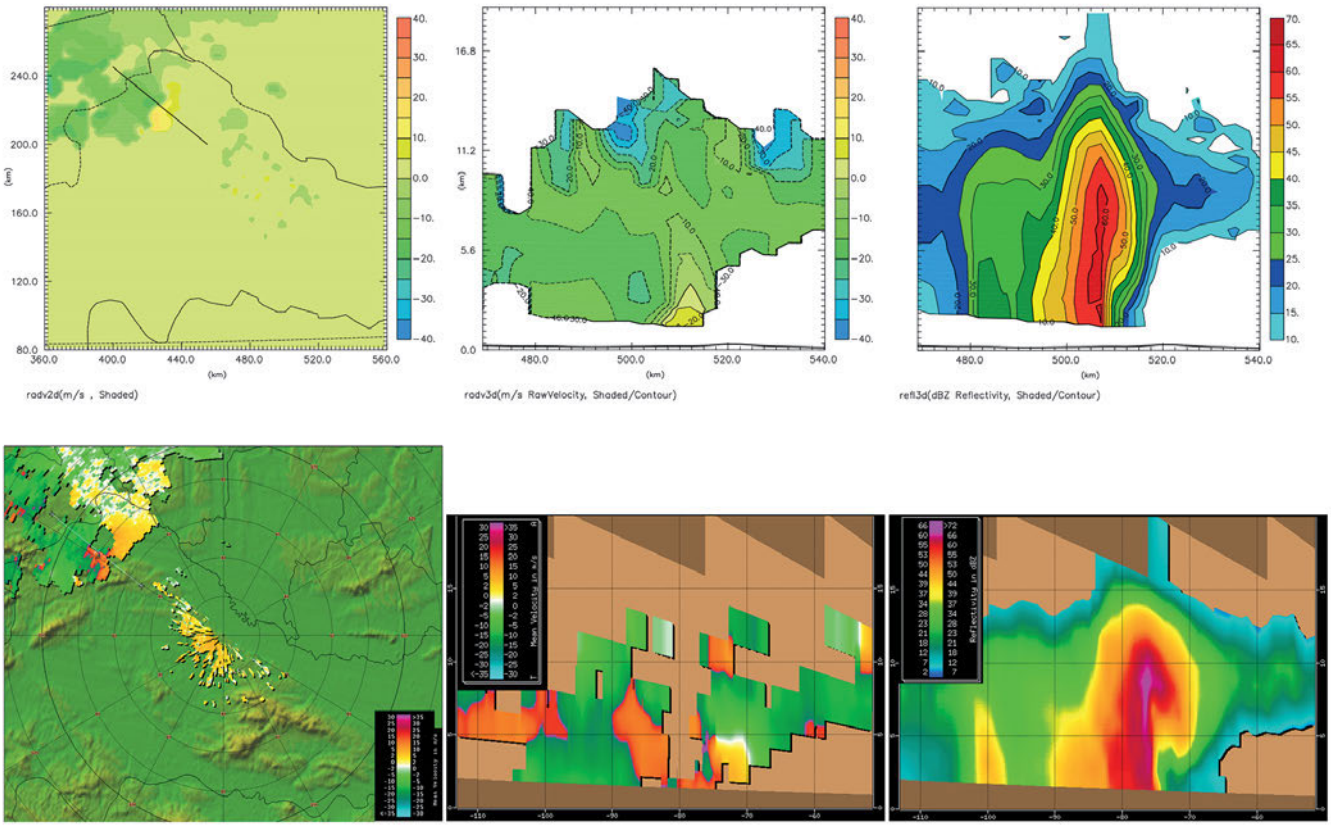

Figure 2: Remapped (first row) and raw radar display (second row) radar data from Bilogora radar at 1915 UTC. First column: radar radial velocity from lowest PPI scan (0.5 °). Black line indicates line of vertical cross-section. Second column: Vertical cross section of radar radial velocity through line indicated at PPI image. Third column: Vertical cross section of radar reflectivity through line indicated at PPI image.

forecast with horizontal resolution of 0.5 ° that was initialized at 1200 UTC 24 June 2008. The Lin (Lin et al., 1983) five-category water and ice cloud microphysical scheme was used. The 1.5-order (turbulent kinetic energy) TKE-based subgrid-scale turbulence parameterization with planetary boundary layer parameterization for unstable boundary layer (Sun and Chang, 1986) was used. The short and long wave radiation package developed at the National Aeronautics and Space Administration (NASA) Goddard Space Flight Center (Chou 1990, 1992; Chou and Suarez 1994) was used. Land surface conditions are predicted using two-layer soil-vegetation model. For convection Kain and Fritsch cumulus parameterization was used in 24 km and 8 km ARPS run. No convective parameterization was applied in the 2.5 km ARPS run. More about dynamical equations and physical parameterizations in the ARPS model can be found in Xue et al. (2000, 2001). In order to investigate the influence of resolution and assimilation of different data types on the quality of the model forecast, a number of experiments were performed; the most important experiments are summarized in Table 1.

The ARPS model with 8 km horizontal grid spacing (ARPS8) was initialized at 1200 UTC 24 June 2008 using initial and hourly lateral boundary conditions (LBC) from ARPS24 and a 9 hour forecast was performed. A nested ARPS model with 8 km horizontal grid spacing was initialized at the same time, used the same initial and LBC but it incorporated hourly sequential data assimilation of SYNOP data (ARPS8-assim) starting from 1500 UTC (thus ARPS8 and ARPS8-assim are the same for first 3 hours of forecast). SYNOP data were assimilated at 1500, 1600, 1700 and 1800 UTC (Fig. 3a). Assimilation of SYNOP data was performed in two steps. First analysis increments were calculated at full hour using as a background forecast from previous cycle. For calculating analysis increments ADAS – ARPS Data Analysis System (Brewster, 1996) was used. ADAS is based on Bratseth method which is successive correction scheme (Bratseth, 1986) that theoretically converges to limit which is optimal in statistical sense (same as optimal interpolation method). The Bratseth method accounts for the relative error between different observation types and the background and in ADAS it can be used in multi-pass strategy where in the first few iterations broad-scale data are used and afterwards in following iterations more detailed data are introduced. In the second step analysis increments were added gradually to background field during model run using the incremental analysis update (IAU) procedure

Table 1: Summary of experiments performed. For assimilation European SYNOP data and radar data from Bilogora radar (Croatia) were used. If SYNOP or radar data was assimilated time of analysis is written.

Experiment name	Horizontal grid spacing [km]	Analysis using SYNOP data	Analysis using radar data	Time of initialization [UTC]	Maximum forecast range	LBC
ARPS24	24	–	–	1200	9 h	GFS
ARPS8	8	–	–	1200	9 h	ARPS24
ARPS8assim	8	1500 UTC, 1600 UTC, 1700 UTC, 1800 UTC	–	1200	9 h	ARPS24
ARPS2.5_ex1	2.5	–	–	1800	3 h	ARPS8
ARPS2.5_ex2	2.5	–	–	1800	3 h	ARPS8assim
ARPS2.5_ex3	2.5	–	1800 UTC 1815 UTC	1800	3 h	ARPS8
ARPS2.5_ex4	2.5	–	1800 UTC 1815 UTC	1800	3 h	ARPS8assim

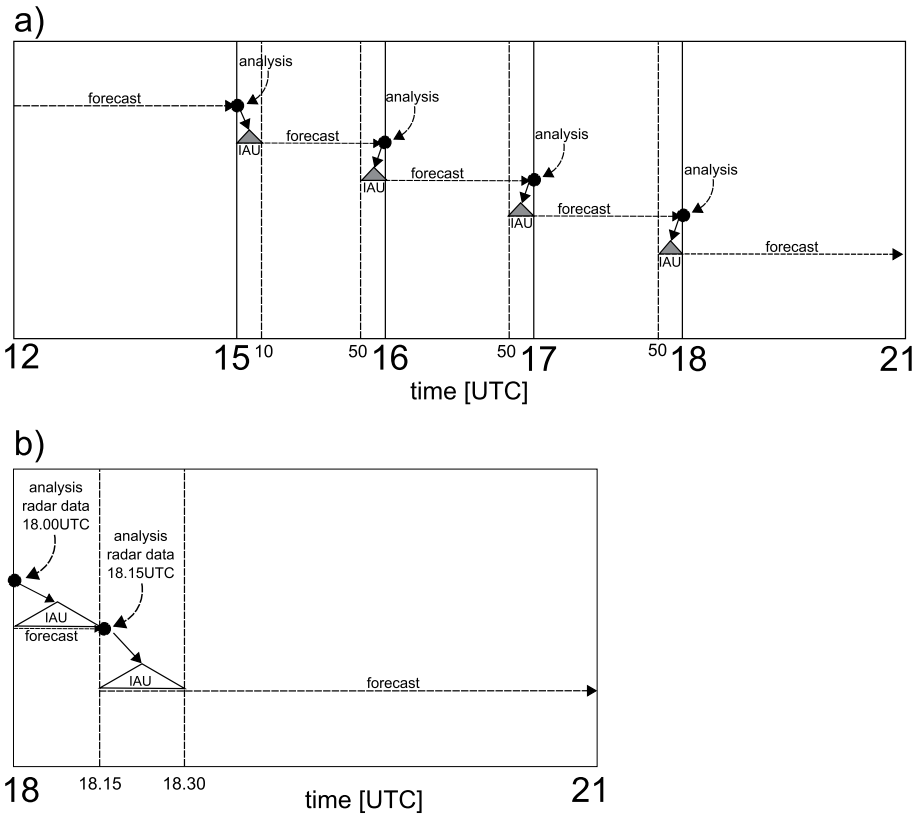

Figure 3: Scheme of data assimilation for ARPS8-assim and ARPS2.5*. a) Assimilation of SYNOP data in ARPS8-assim at 15, 16, 17 and 18 UTC. Analysis increments were calculated using ADAS at full hour and added to the model using IAU with time interval of 10 min starting at 1500 UTC, 1550 UTC and 1650 UTC, 1750 UTC. b) Assimilation of radar data in ARPS2.5*. Increments were calculated at 1800 UTC and 1815 UTC using radar data and added to the model using IAU with time interval of 15 min.

(Bloom et al., 1996) within a time interval of 10 minutes. IAU is a procedure where analysis increments are gradually added to the model during model integration for a defined time interval allowing for unobserved variables to adjust while reducing data insertion noise in the model forecast.

As indicated at Fig. 3a at 1500 UTC 3 hour forecast (ARPS8) was used as the background for the first analysis. The model was than restarted and a 1 hour forecast was performed with IAU during first 10 minutes of model run. This forecast was used as background for analysis at 1600 UTC but this time model was restarted

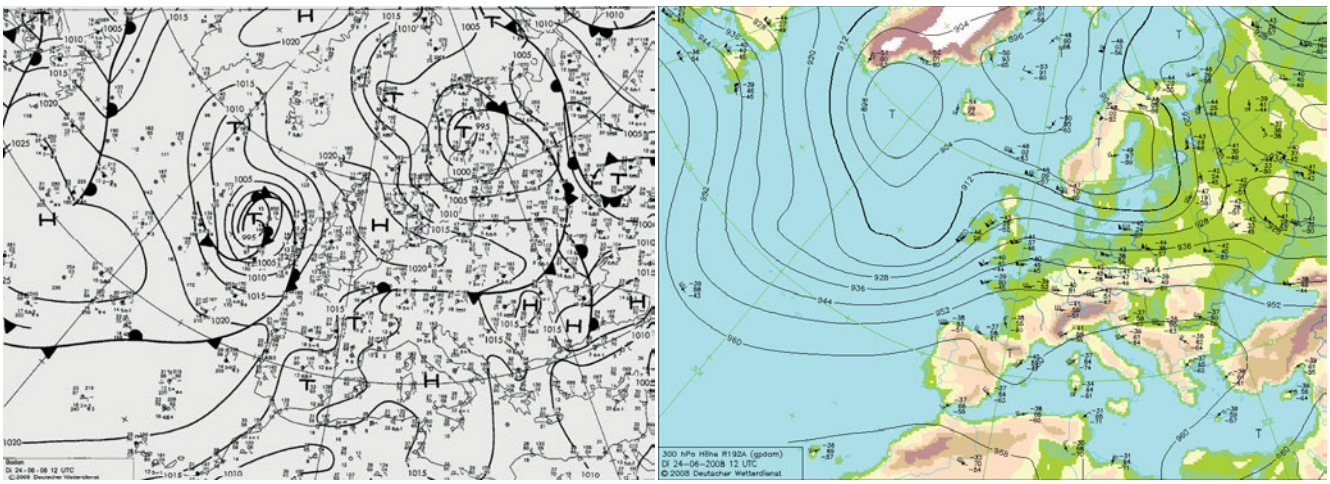

Figure 4: Left: DWD (Deutscher Wetterdienst; Germany's National Meteorological Service) surface analysis at 1200 UTC 24 June 2008. Thick contours represent surface pressure in hPa. Fronts are marked by standard symbols. Right: 300 hPa DWD analysis for 24 June 2008, 1200 UTC (data from radiosonde measurement). Geopotential height (contours, gpdm) and wind barbs.

at 1550 UTC and forecast until 1700 UTC was performed with IAU during first 10 minutes of model run (the assimilation of surface data in 10 minutes before the top of the hour is preferred because most SYNOP observations are actually made before the hour). Same was repeated for analysis at 1800 UTC but this time forecast was performed from 1750 until 2100 UTC. All of the highest resolution runs (ARPS2.5*; * denotes different configurations) were initialized at 1800 UTC 24 June 2008. Using ARPS8* output, for initial and lateral boundary conditions (half-hour coupling frequency). Initialization time of ARPS2.5* km runs was chosen at 1800 UTC as at that time the first convective cells came close enough to the Bilogora radar to be detected in its lowest radar scan. The maximum forecast range of these simulations is rather short but the main focus of this study was put on high-resolution model initialization and simulation of cell life in period of its most intense development.

Radar data was assimilated in ARPS2.5_ex3 and ARPS2.5_ex4 sequentially at 1800 and 1815 UTC (Fig. 3b). As a background for radar data assimilation at 1800 UTC the ARPS8* forecast valid at same time and interpolated to ARPS2.5* grid was used. Assimilation of radar radial winds was performed using three-dimensional variational analysis (3DVAR; Gao et al., 2004), while radar reflectivity data increments were calculated through a cloud analysis procedure where hydrometeors and cloud fields are defined, and adjustments to the in-cloud temperature and moisture fields are made (Brewster, 2002). Analysis increments were added to the background field during a 15 minute model run and using IAU with a 15 minute window. This 15 minute forecast was used as background field for calculating increments for 1815 UTC analysis. Analysis increments were added to background field using 15 minute IAU during ARPS2.5* forecast that started at 1815 UTC and ended at 2100 UTC.

3 Observational analysis of the severe storm

3.1 Severe-storm event overview

A severe thunderstorm hit the northwestern part of Croatia in the late afternoon and evening of 24 June 2008. Strong wind gusts and hail were observed, and there were even reports of a small tornado. Hail was the size of a hazelnut (~ 13 mm) or in some locations the size of an egg (~ 50 mm). The storm caused significant damage to crops, buildings and cars. One insurance company published that an amount of ~ 5.3 million EUR was paid to the insured persons in Croatia due to damage claims from this event. The storm was initiated near Graz in Austria and traveled southeast through Slovenia and Croatia reaching as far as Bosnia and Herzegovina. The storm moved to the southeast at a speed of about 20 m/s.

3.2 Synoptic environment

The atmosphere around Croatia in the month of June 2008 was very unstable with a number of storms affecting Croatia. Very warm temperatures (~ 32 °C) had been measured on 22 and 23 June. The DWD (Deutscher Wetterdienst; Germany's National Meteorological Service) surface analysis at 1200 UTC 24 June indicated the surface pressure over Croatia was high with little pressure gradient (Fig. 4). A pronounced surface low was located west of the British Isles and it moved NE during the next day thus supporting warm air advection over France and Germany. A front was located north of the Alps and it slowly moved to the east during next 12 hours.

At upper levels (300 hPa, Fig. 4) pronounced low pressure system was present near Scandinavia while an upper level ridge was located over the Mediterranean sea with margin located south of Alps. There was a weak

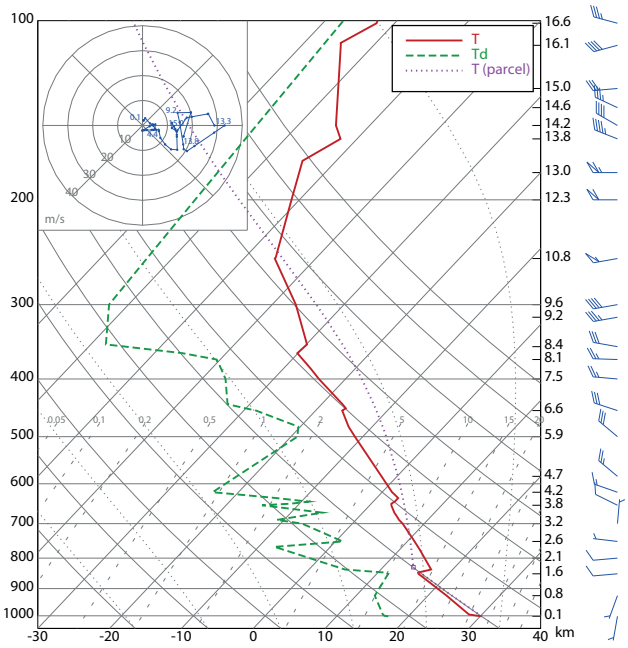

Figure 5: Zagreb-Maksimir sounding on 1200 UTC 24.06.2008, skew *t*-log *p* graph. Full red line is temperature, while green dashed line is dew point. Dotted purple line is virtual temperature of the surface parcel. Wind speed is given in knots. The hodograph is shown in inset, upper left.

shortwave trough over Pyrenees so the area downstream (east) of it was supportive for rising motions.

DWD analyses (not shown) indicate that flow at upper levels north of Alps was gradually changing from SW to W during the day 24 June 2008. South of the Alps, due to the location of the margin of the upper level ridge, the upper level flow had a southerly component. At and above the 500 hPa level cold air was advected southward to the area west and over the Alps between 1200 and 1800 UTC. At lower levels southwesterly winds advected warm moist air to the area around the Alps. The combination of increasing humidity and temperature at lower levels with advection of cold air at upper levels caused destabilization of atmosphere.

3.3 Mesoscale features

The sounding location closest to the point of the storm's entrance into Croatia is Zagreb-Maksimir located approximately 70 km SW of that point (Fig. 1). Fig. 5 shows the Zagreb-Maksimir sounding at 1200 UTC 24 June 2008, which is 6 hours before the storm entered Croatia.

At that time the atmosphere at Zagreb at low levels was fairly dry (10–12 g/kg), with a nearly dry-adiabatic lapse rate below 1.5 km. Vertical profiles of measured temperature and dew point temperature indicate that the atmosphere was potentially unstable. CAPE computed using the virtual temperature of the surface parcel was moderate with value of 1261 J/kg and CIN had value of − 11 J/kg. For other stability parameters Showalter was negative (−6) which indicates increased likelihood of showers and thunderstorms (Showalter, 1953). The Showalter index is calculated as algebraic difference between environmental temperature at 500 hPa and temperature an air parcel has after being lifted from 850 hPa dry-adiabatically to LCL and then moist-adiabatically to 500 hPa. Severe Weather Threat Index (SWEAT) which incorporates instability, wind shear, and wind speeds information had value 196 which is at the low end of values indicating some potential for supercell formation (Miller, 1972).

In the first three kilometers pronounced directional wind shear was present but with wind speeds being very small. Above that wind shear increased due to the presence of the upper level jet stream at around 13 km. Veering winds are noted in the first 6 kilometers.

Fig. 6 shows ARPS8-assim model fields at 1600 UTC 24 June 2008. At the surface the wind had speed up to 5 m/s with south or south-west direction south of Alps and north or north-east direction north of Alps. A convergence line had formed as indicated by the positive surface moisture flux convergence contours and it is located north of Austria-Slovenia border. A somewhat weaker convergence line can be found in Slovenia. At upper levels strong north-west (500 hPa) and west (300 hPa) wind were present. When plotted over the temperature field they indicate cold temperature advection in the region over and north of Slovenia.

Advection of moisture at low levels and cold air advection at upper levels destabilized the atmosphere surrounding the Alps. Due to the upper level flow, air parcels moved up over the Alps which initiated development of convective cells on the lee side of the Alps. Around 1615 UTC deep convection was initiated NW of Graz. A mesoscale convective system (MCS), consisting of one dominant storm and a few smaller cells, developed and moved SE. At 1800 UTC the MCS was located near the Austria-Slovenia border, with the most-developed cell having reflectivity greater than 60 dBZ (Fig. 7a). After the MCS entered Slovenia the most-developed cell started to exhibit rightward propagation and had a three-body scatter spike on radar, indicative of hail. From 1900–l915 UTC the main cell developed supercell characteristics such as weak echo region (WER) and bounded weak echo region (BWER) (Fig. 7b, 7c, 8). At 1915 UTC the storm hit the town of Varazdin, where strong winds and hail caused great damage (Fig. 7c). After that, the storm cell split with the left-moving cell dissipating and the right-moving cell continuing to develop (Fig. 7d). At 2100 UTC (Fig. 7e) the storm began to weaken, but later strengthened again at the Croatian-Bosnian border.

Fig. 8 depicts the observed radar reflectivity field at 0.5 ° elevation of the Bilogora radar taken at 1920 UTC, which is approximately when the storm hit Varazdin. At that time the main cell was already well developed. The updraft was located on the front flank of the storm where both WER and BWER are found. In the raw radial ve-

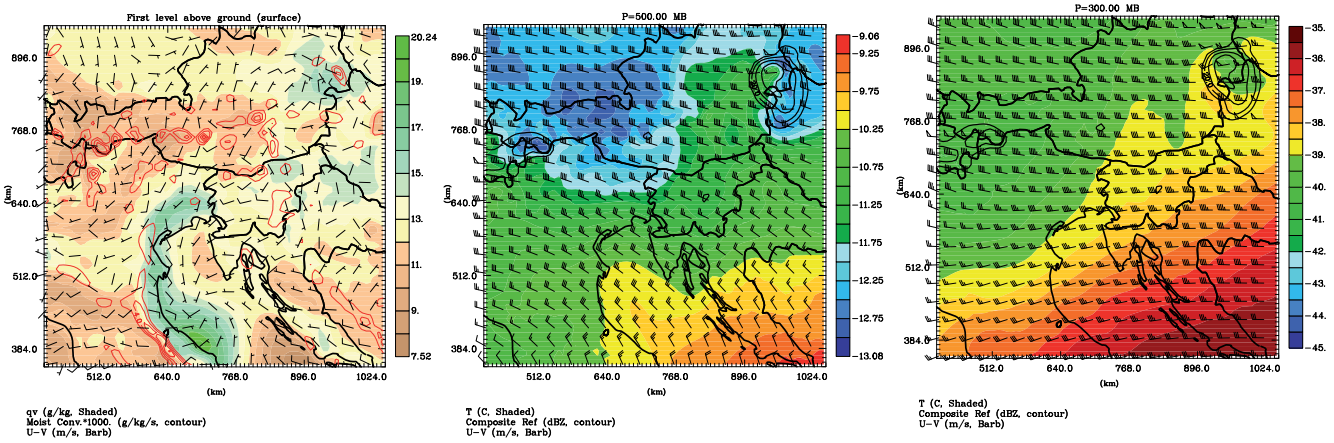

Figure 6: Model fields from ARPS8-assim at 1600 UTC 24 June 2008. Left: Surface (10 m above ground level) water vapor mixing ratio (shaded) in g/kg. Surface moisture flux convergence in g/kg/s $*$ 1000 with only positive values shown (red contours). Middle (300 hPa) and right (500 hPa): Temperature in °C (shaded). Composite reflectivity (maximum reflectivity in given model column) in dBZ (black contour) with values greater than 20 dBZ plotted. Wind barbs (half barb = 2.5 m/s; full barb = 5 m/s).

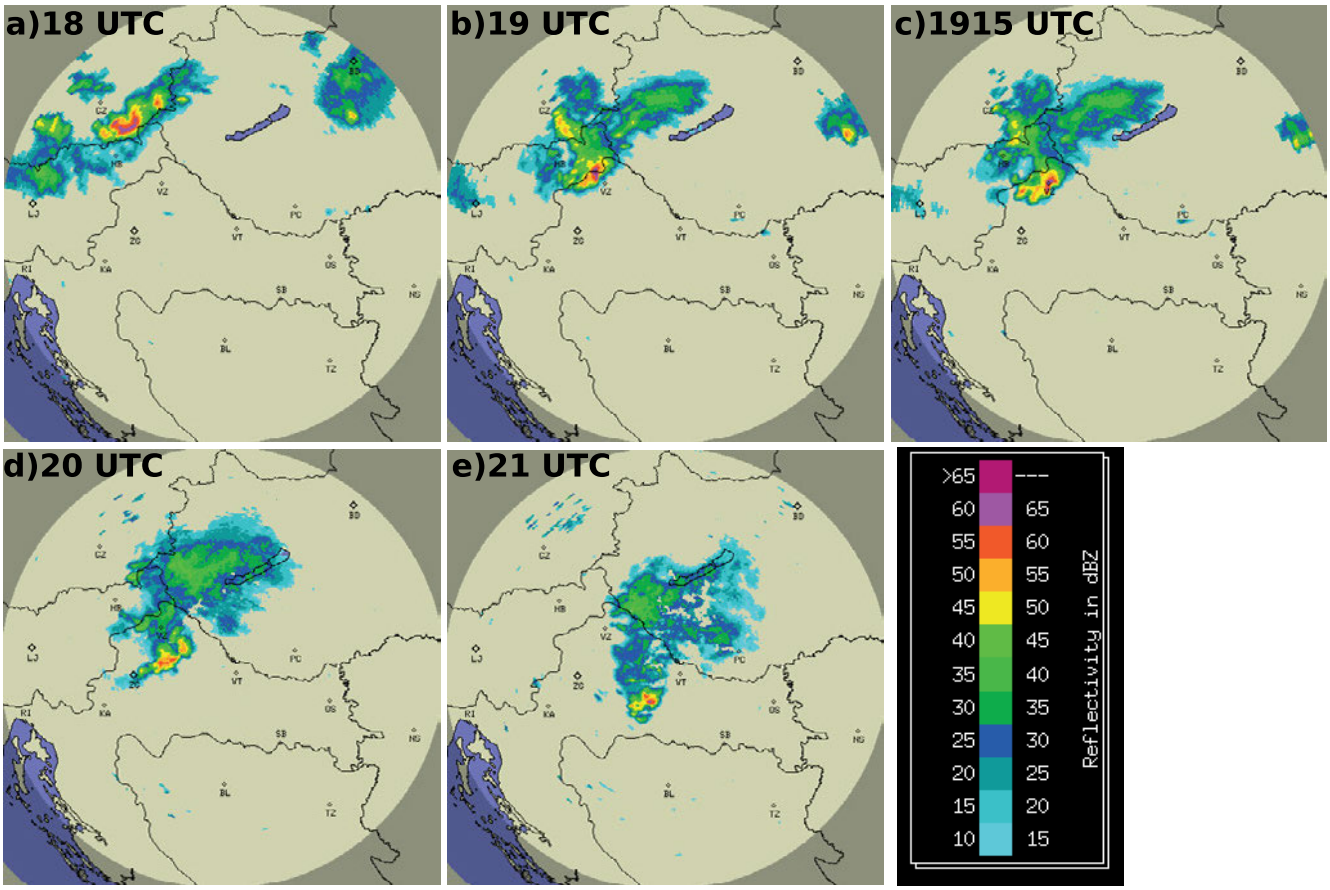

Figure 7: Radar reflectivity on CAPPI display at 2 km from Bilogora radar for 24 June 2008 and for specific times between 1800 UTC and 2100 UTC. Colors are reflectivity in dBZ. Maximum radar range indicated by lighter background is 240 km. Location of town Varazdin is denoted with letters VZ.

locity observations (not shown) no mesocyclone can be identified, but this could be due to low Nyquist velocity (16.5 m/s) and subsequent aliasing. Nevertheless, aliasing was removed from remapped data (Fig. 2; middle column) and there between 1.5 and 3.5 km in vertical and 495–515 km in x direction a mesoscale vortex can be identified which cloud be a descending mesocyclone. Some indications of mesocyclone were also present in remapped radar radial velocity data at 1900 UTC (not shown) but due to wide gaps in observed radial velocity data wide gaps are also present in remapped radar data so existence of mesocyclone could not be confirmed.

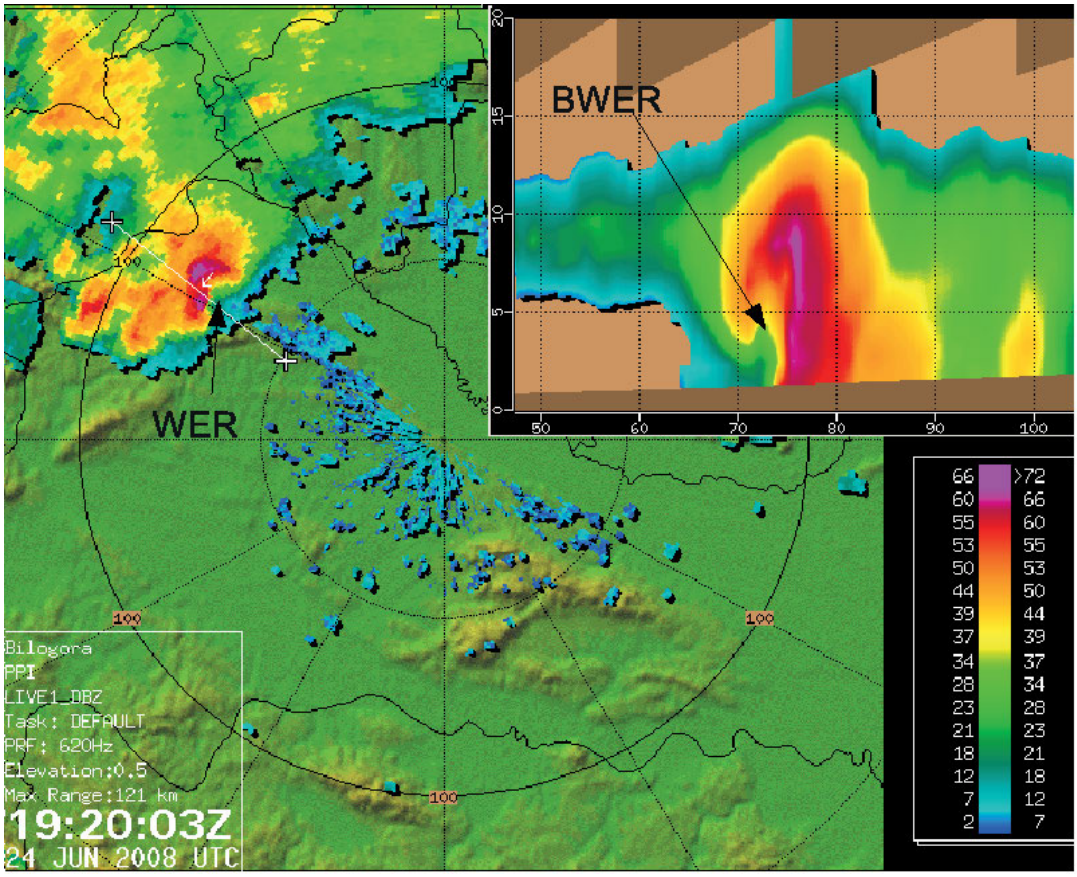

Figure 8: Observed radar reflectivity field at 0.5 ° elevation of the Bilogora radar at 1920 UTC. In the upper right corner a vertical cross section of radar reflectivity taken along white line indicated at PPI scan is shown. Location of WER and BWER are indicated with black arrows.

4 Modeling results

In order to investigate the impact of model horizontal grid spacing and data assimilation on the ability of the numerical model to represent storm motion and development, a number of different model configurations were tested. Horizontal grid spacing of 8 km is too coarse to properly represent a small scale convective storm but since this case had some broader convection activity some features should be represented. Additionally, to enhance initialization of the 8 km model, assimilation of surface measurements was conducted as described in Section 2. Fig. 9 depicts the model simulated reflectivity at 2 km height for the period 1800–2000 UTC for the 8 km model run without data assimilation (ARPS8) and the 8 km model run with assimilation of synoptic measurements (ARPS8-assim). Comparing those results with the observed radar images (Fig. 7) it can be seen that at 1800 UTC ARPS8 had a weak storm located north of the location of the observed storm. The modeled storm moved to the east until 1900 UTC and southeast thereafter. At 1800 UTC ARPS8-assim had a well-developed storm in the proper location; at 1900 UTC the modeled storm was at Slovenia-Croatia border, and at 2000 UTC the storm was located south of Varazdin. Therefore, movement of the storm system was better described with the ARPS8-assim run as it started to move southeast one hour before ARPS8, in accordance with the radar observation. Also the simulated reflectivity at 2 km was stronger in the in ARPS8-assim run compared to ARPS8, and the reflectivity is in better agreement with radar observations.

Fig. 10 shows comparison of surface fields from ARPS8 and ARPS8-assim model. In the ARPS8-assim high values of CAPE (above 3000 J/kg) are present over the area covering Slovenia and northern part of Croatia with very strong CAPE gradients along the right hand side of greatest modeled CAPE. Higher negative values of CIN (more than 250 J/kg) can be noticed on area over Hungary. On the other hand, ARPS8 model has even larger values of CAPE over Slovenia but much smaller values over northern part of Croatia (up to 2000 J/kg). CIN values in northern part of Croatia are higher than in ARPS8-assim run while they are lower in area over Hungary. Surface winds in both runs were rather weak (less than 5 m/s) except near convective cells indicated by contours of composite reflectivity. More moisture was present in surface fields of ARPS8-assim over Croatia and Slovenia than in the ARPS8 run. Wind at upper levels (not shown) had mainly a WNW direction up to 10 km and it was similar in both runs except for places where convective cells were present.

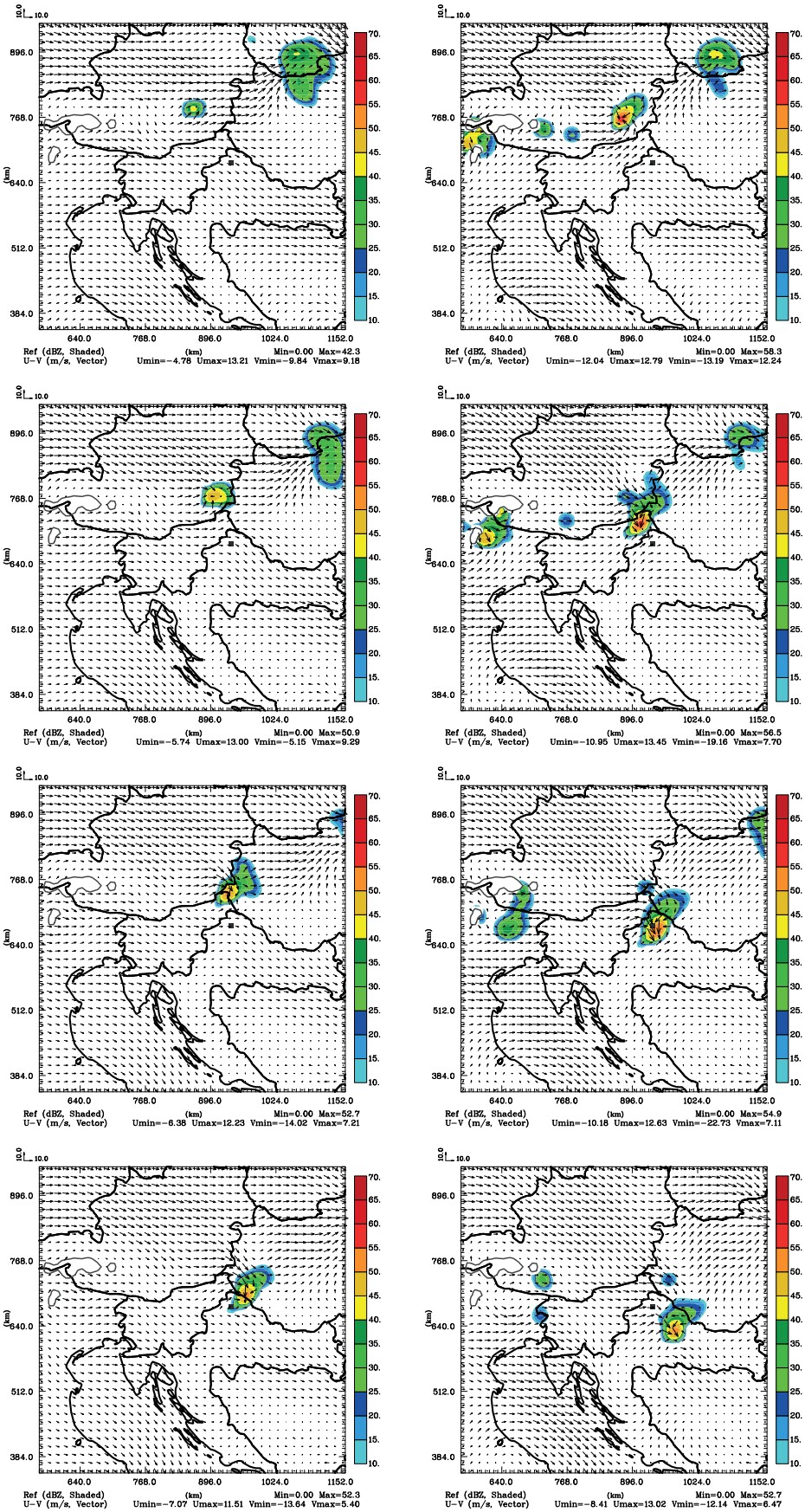

Figure 9: Simulated radar reflectivity at 2 km height (color, in dBZ) from ARPS8 (left) and ARPS8-assim (right) every hour from 1800 until 2100 UTC. Also total wind field at 2 km height is shown, scale in m/s at bottom left. With black square location of town Varazdin is denoted. Thin black contours indicate areas where the wind cannot be computed (terrain height above 2 km).

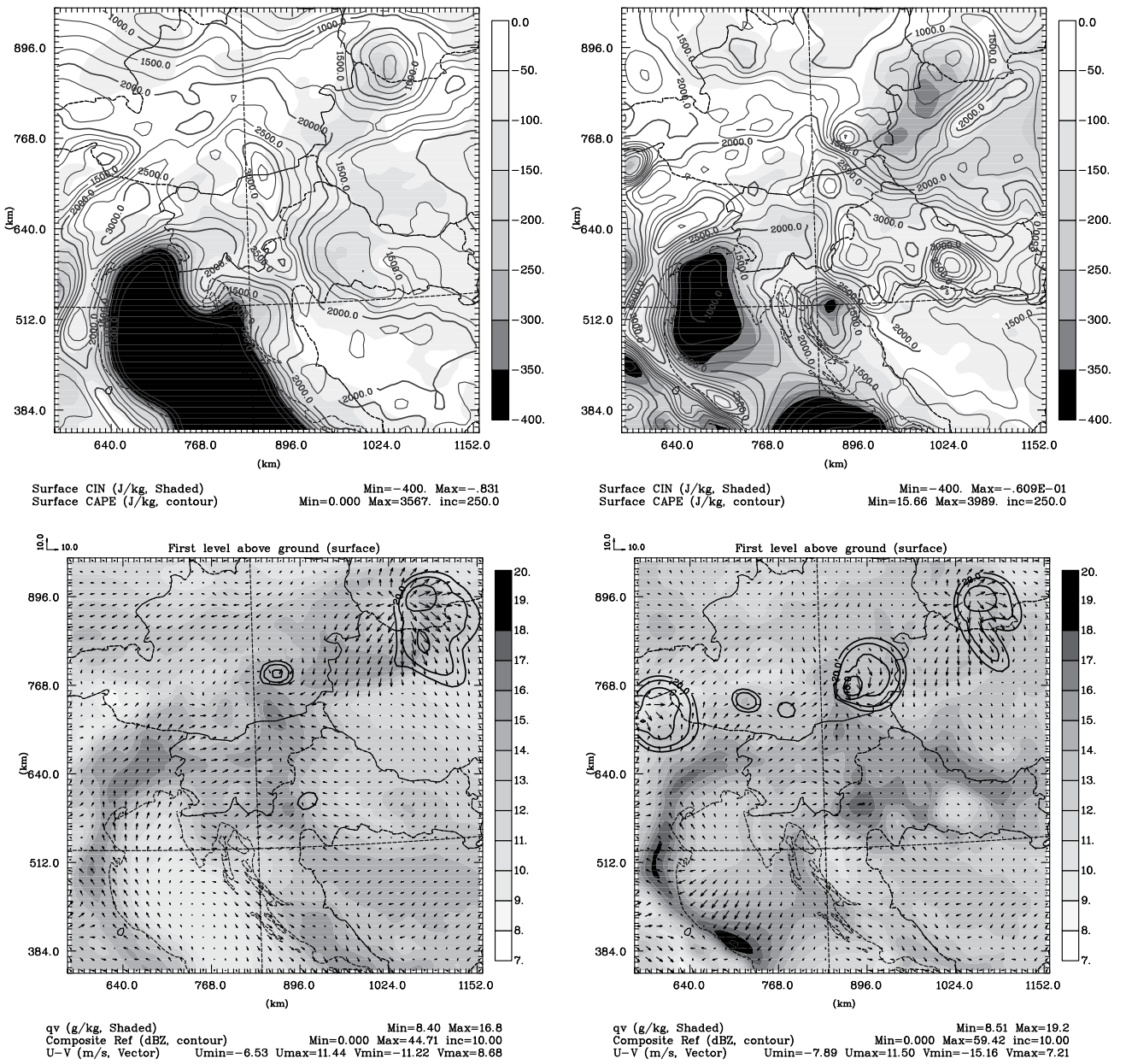

Figure 10: Portion of ARPS8* domain showing surface fields plotted from ARPS8 (left) and from ARPS8-assim (right) forecast valid at 1800 UTC 24 June 2008. First row: Surface convective inhibition – CIN (shaded; J/kg). Surface convective available potential energy – CAPE (grey contours; J/kg). Second row: Surface (10 m above ground level) water vapor mixing ratio (shaded; g/kg). Composite reflectivity (maximum reflectivity in given model column) in dBZ (black contour; dBZ) with values greater than 20 dBZ plotted. Surface wind (wind vectors; every second grid point; m/s).

Movement of the storm in both runs can be explained using these surface patterns and vertical wind shear. In ARPS8-assim convective cell near Slovenia-Austria border at 1800 UTC was already well developed (maximum simulated reflectivity at 2 km height more than 50 dBZ) and its subsequent motion was driven by heterogeneous environmental conditions. The steering wind had mostly a westerly direction but east of the convective cell location an area of strong CIN was present while south of there was an area of high CAPE values and increased surface moisture. Additionally, winds in pseudo-soundings from both ARPS8* models at location of Varazdin (not shown) are quite similar to the one in the sounding from Zagreb Maksimir (Fig. 5) with veering winds in first few kilometers that support rightward propagation of supercell storm. Thus this resulted in SE motion of the convective cell. On the other hand the convective storm in ARPS8 run was located far north than in ARPS8-assim and it was not as well developed (maximum simulated reflectivity at 2 km height ~ 40 dBZ). In first 1–2 hours it was moving east following the steering flow until it was more developed and

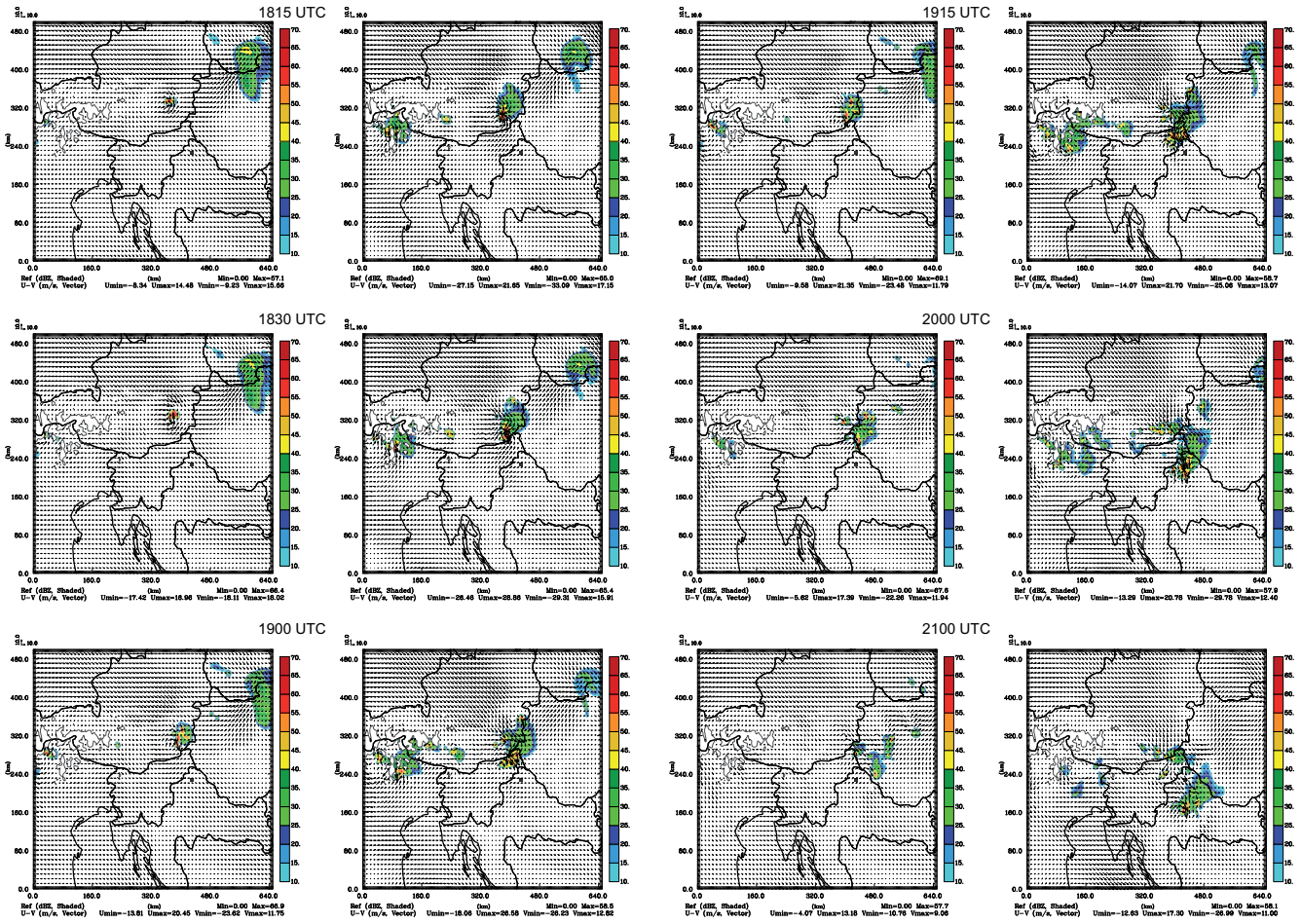

Figure 11: Simulated radar reflectivity at 2 km height (dBZ, colors) at 2 km for ARPS_ex1 (left) and ARPS_ex2 (right). Reflectivity is plotted for 1815, 1830, 1900, 1915, 2000 and 2100 UTC. Also total wind field at 2 km height is shown, scale in m/s at top left. The location of the town of Varazdin is denoted by the black square. Thin black contours indicate areas where the wind cannot be computed (terrain height above 2 km).

then it began to move toward the SE. It is noted that in both runs the track of the storm is collocated with an area of large CAPE gradients along the right-hand side of the area of greatest modeled CAPE.

To improve simulation of storm development two high resolution runs ARPS2.5_ex1 and ARPS2.5_ex2 were performed where for initial and boundary conditions respectively ARPS8 and ARPS8-assim were used. Simulated reflectivity at 2 km height at specific times between 1800 and 2100 UTC are shown in Fig. 11 (timing is selected to show an overview of storm development in first 45 minutes and the period of storm development and propagation for the time periods matching Fig. 7).

In both runs the initial storm near Slovenia-Austria border was rapidly enhanced compared to the ARPS8 runs which are noted by the increase in simulated reflectivity, up to 10 dB, in the first 15 minutes of the high-resolution simulation. Movement and location of the convective system in both runs closely followed that of the outer mesoscale model. Still, in the high resolution simulation the original storm was decomposed in number of smaller ones which was more pronounced in ARPS2.5_ex2 simulation. Storm decomposition into number of small storms started after 30 minutes of high resolution-simulation in ARPS2.5_ex2 and half hour later in ARPS2.5_ex1. At 1915 UTC, which is the time when storm hit town Varazdin, main storm in ARPS2.5_ex2 was located 30–40 km north of the observed location while in ARPS2.5_ex1 it still had not entered Slovenia. At the end of simulation there is much better agreement with the observed radar image in the ARPS2.5_ex2 run, where three main storms were located in middle of northern Croatia. Nevertheless, the location was far north from observed one and some spurious storm cells were present over the NE part of Slovenia. Also the structure of storm was not well captured as small values of observed reflectivity over Hungary were not simulated.

To improve the initialization of the high-resolution simulation, radar data assimilation was used as described in Section 2.2.A. A comparison between high-resolution simulation using ARPS8 as background field for radar data assimilation and as boundary condition (ARPS2.5_ex3) versus high-resolution simulation using ARPS8-assim for same (ARPS2.5_ex4) is shown in Fig. 12. Radar data assimilation was performed in two

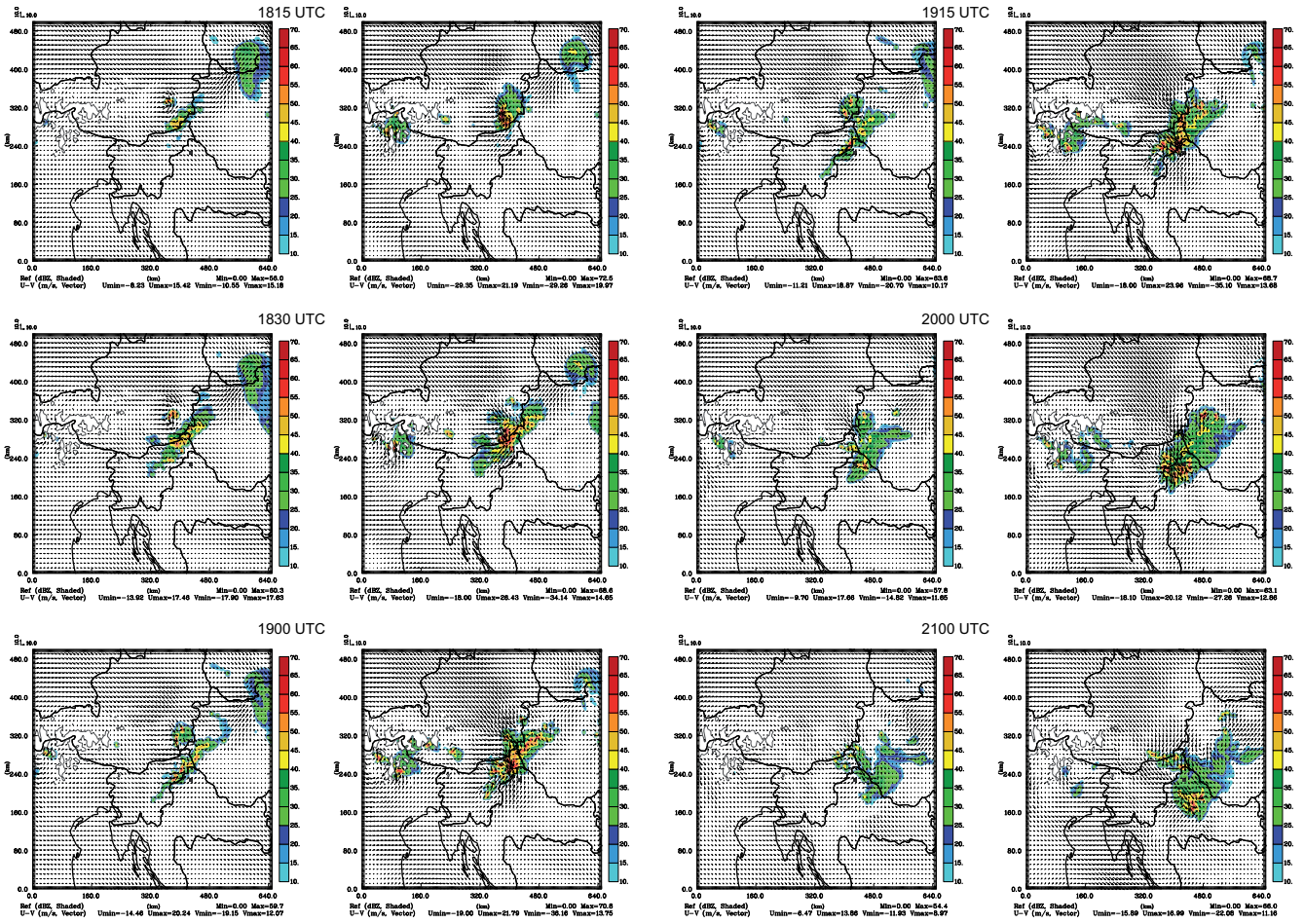

Figure 12: Simulated radar reflectivity at 2 km height (dBZ, colors) at 2 km ARPS_ex3 (left) and ARPS_ex4 (right). Reflectivity is plotted for 1815, 1830, 1900, 1915, 2000 and 2100 UTC. Also total wind field at 2 km height is shown, scale in m/s at top left. The location of the town of Varazdin is denoted by the black square. Thin black contours indicate areas where the wind cannot be computed (terrain height above 2 km).

intermittent cycles in first half hour of high-resolution simulation and this is evident in simulated reflectivity fields at 2 km height. In ARPS2.5_ex3 radar data assimilation led to generation of an additional storm located SE of the one present in the background state. Those two storms were developing almost independently one of other until 1900 UTC when the original storm encountered an area affected by passage of the newly-generated storm. After that radar data assimilation newly generated storm was soon decomposed into a number of smaller storm cells but eventually most of them decayed leaving the one dominant storm cell that moved SE until the end of simulation. At 2100 UTC a storm of very weak intensity in the simulated reflectivity was located in the northern part of Croatia and also some small spurious storm cells were present at NE part of Slovenia. The initial storm cell in ARPS2.5_ex4 had a location a bit north of the location where the radar assimilation procedure generated a new storm cell. Those two storm cells interacted forming wide band of high reflectivity and it continue to move SE until the end of our simulation. At 1915 UTC the main storm cell was located near town Varazdin, very close to the observed one but about 15 minutes late. At the end of simulation main cell was located at similar location as in ARPS2.5_ex2 experiment but with better storm structure having low reflectivity in the part extending over Hungary and thus providing the best results from all simulations performed.

To go beyond the rather subjective verification based on comparison of model simulated reflectivity and observed radar CAPPIs an objective verification was performed. Equitable threat scores (ETS; Schaefer, 1990) of predicted composite radar reflectivity were calculated for 5, 15, 30 and 45 dBZ thresholds (Fig. 13). Scores were calculated for times shown at Figs. 11 and 12 except for 2000 UTC as there was a problem with the radar data so the score was calculated at 2015 UTC. Similar to conclusions drawn from the subjective verification, the highest scores for all thresholds were obtained for the ARPS2.5_ex4 experiment. Experiments with radar data assimilation have higher ETS values for all thresholds and almost all times compared to those without radar data assimilation. The increase in ETS after the first 15 minutes of simulation is due to IAU procedure of adding analysis increments. Very small values of ETS for 45 dBZ threshold are partially due to limi-

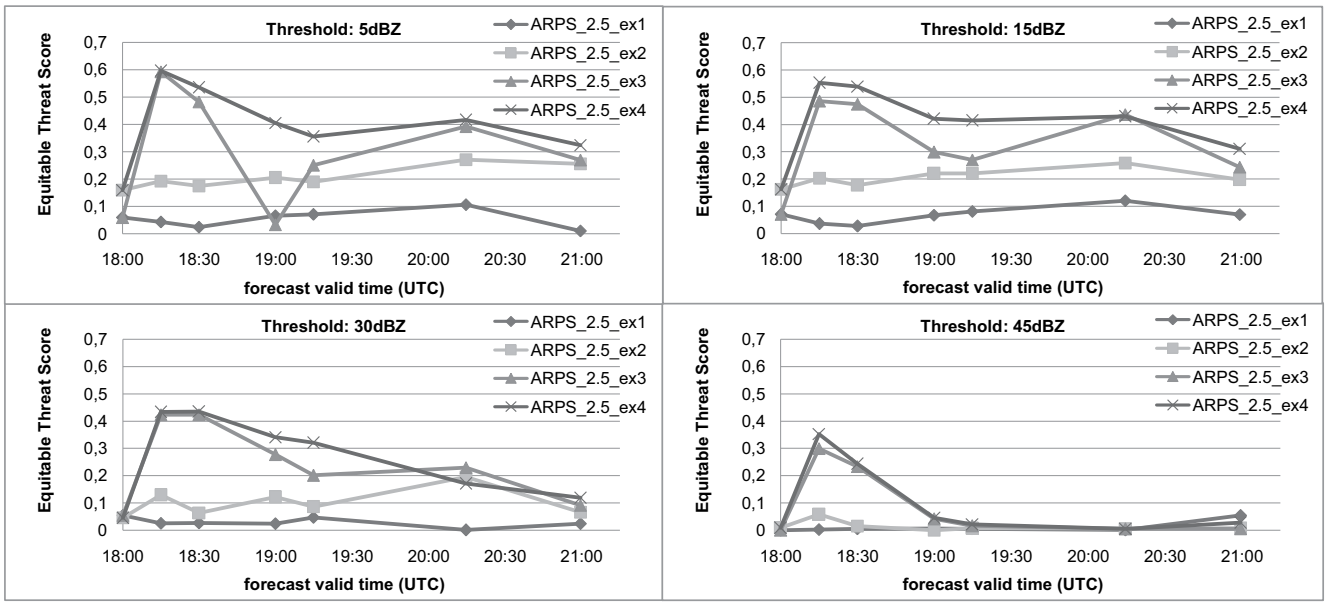

Figure 13: Equitable threat scores (ETS) of predicted composite reflectivity for 5, 15, 30 and 45 dBZ threshold values from experiments ARPS2.5_ex1, ARPS2.5_ex2, ARPS2.5_ex3 and ARPS2.5_ex4. ETS was calculated for 1800, 1815, 1830, 2015 and 2100 UTC.

tations of ETS calculations for models with small horizontal grid spacing and small scale structures that are being verified. In such cases even if the forecast of storm structure is rather well, a position error can lead to very low ETS (e.g. Dawson et al., 2006). Fig. 14 shows results of ARPS2.5_ex4 model simulation and remapped radar data valid at 1915 UTC. Simulated reflectivity at 4 km height shows that shape of storm structure was captured reasonably well except for the erroneous storm cells on the rear flank of the convective system. The vertical cross section indicates that in model simulation broader and less intense updraft area is present with vertical velocity reaching up to 14 m/s. Also the location of strongest radar reflectivity pattern was missed by ~ 30 km in this specific cross-section.

5 Summary and conclusions

In this paper analysis and numerical simulation of one severe storm event in Croatia are presented. The event was described using observational data and a number of numerical simulations of the event were performed. The model simulations were performed with different model setups to test the influence of horizontal grid spacing and impact of assimilation of conventional and high resolution (radar) data. The results showed that the assimilation of both conventional and radar data have a positive impact in forecasting storm development and movement. This is true at both model resolutions, one with 8-km horizontal grid spacing and one with 2.5-km horizontal grid spacing. Results suggest that it is important to have a properly modeled environment in the forecast model driving the lateral boundary conditions for the high resolution run, i.e., an environment that is supportive of convection processes is necessary. In ARPS8-assim run assimilation of surface observations provided low level ingredients (surface moisture, convergence lines) needed for convection initiation and further storm propagation. Broad areas of high values of CAPE covering Slovenia and northern parts of Croatia on one side and larger values of CIN over Hungary on the other side resulted in a southeastward storm motion which is comparable with radar observations. Enhancing the horizontal grid spacing of the model to 2.5 km did not change the overall behavior of the simulated convective system much. The intensity of the storm was enhanced but the movement was still dictated by the initial environment and LBC of the driving model. An environment that is not supportive of storms in the outer grid model can be problematic even if the inner grid model has small horizontal grid cell spacing and assimilates data with high temporal and spatial resolution. Results from this case show that even if a storm-scale model is used and radar data are assimilated, the storm was not represented well because the driving model has not established a proper environment for storm development. Assimilation of radar data on the inner grid "forced" development of a storm but in subsequent moments the original big storm was decomposed into number of smaller cells in a broad convection area and after entering Croatia it began to quickly dissipate. On the other hand, if the driving model sets up environment that resembles reality, the model with smaller horizontal grid spacing and assimilation of radar measurements can enhance prediction of storm development. Comparison of simulation and observed storm at location near the town of Varazdin (when the observed storm was in its most intense phase) shows that model is able to represent storm structure reasonably well but also it suffers from a few deficiencies. The storm was improperly positioned with a broader and less-intense updraft and also

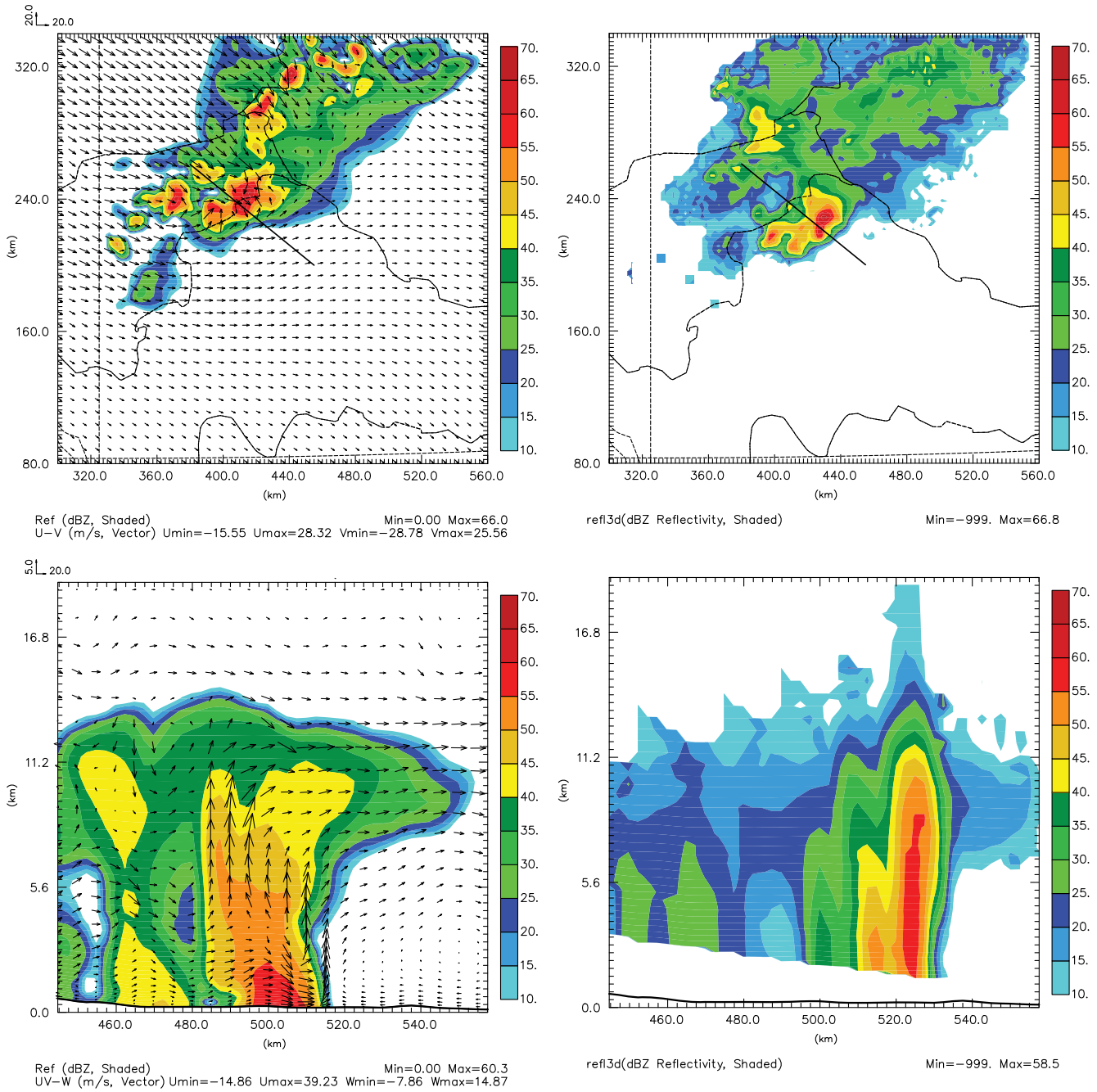

Figure 14: Simulated radar reflectivity from ARPS2.5_ex4 (left) and observed (right) remapped radar reflectivity in dBZ at 4 km height (top row) and vertical cross section through (bottom row) black line indicated at horizontal slice at 1915 UTC 24 June 2008. For model simulation total wind field is shown, scale in m/s at top left. The location of the town of Varazdin is denoted by the black square.

with spurious storm cells at rear flank of convective system. Those could be result of imbalances between different variables that were introduced in the assimilation procedure that triggered the sequence of generation and dissipation of small storm cells. Therefore one has to be careful in how to properly add radar measurement information to model without adding undo noise. Cloud analysis and IAU seams as a good choice, as it gradually adds information to model and changes model environment to be supportive to added moisture modeled from the radar reflectivity via the cloud analysis. Nevertheless, there is room for improvement in this process and it could include more frequent updates in a cycled-mode that can help to force model to act in accordance to measurements (only two updates were used in this study). Furthermore, there are now more sophisticated microphysics options that might more accurately model the storm.

In order to enhance numerical simulation additional steps could include assimilation of data from more radar sites, decreasing horizontal grid spacing to 1 km and/or using multi-moment bulk microphysical parameterizations (e.g. Milbrandt and Yau, 2005a, 2005b). All these steps would increase the computational time and,

depending on the computing resources available, will decrease the lead time for usable forecasts.

Still without these enhancements, the best simulation, in which data assimilation of surface observations set up proper environment in driving model and assimilation of radar observations enhanced small scale features and broader storm structure, the model predicted storm development and movement reasonably well for a few hours when compared to the observed storm.

Acknowledgments

This research was supported by the Meteorological and Hydrological Service (DHMZ) of Croatia and the Center for Analysis and Prediction of Storms, University of Oklahoma. I wish to acknowledge the help provided by office colleagues (Kristian Horvath, Tomislav Kovacic and Stjepan Ivatek-Sahdan) and two anonymous reviewers whose comments improved the original manuscript.

References

Bloom, S.C., L.L. Takacs, A.M. da Silva, D. Ledvina, 1996: Data assimilation using incremental analysis updates. – Mon. Wea. Rev. **124**, 1256–1271. DOI: 10.1175/1520-0493(1996)124<1256:DAUIAU>2.0.CO;2.

Bratseth, A.M., 1986: Statistical interpolation by means of successive corrections. – Tellus A **38**, 439–447. DOI:10.1111/j.1600-0870.1986.tb00476.x.

Brewster, K., 1996: Application of a Bratseth analysis scheme including Doppler radar data. – Preprints, 15th Conf. on Weather Analysis and Forecasting, Norfolk, VA, Amer. Meteor. Soc., 92–95.

Brewster, K., 2002: Recent advances in the diabatic initialization of a non-hydrostatic numerical model. – Preprints, 15th Conf on Numerical Weather Prediction/21st Conf. On Severe Local Storms, San Antonio, TX, Amer. Meteor. Soc., CD-ROM, J6.3.

Brewster, K., M. Hu, M. Xue, J. Gao, 2005: Efficient assimilation of radar data at high resolution for short-range numerical weather prediction. – In World Weather Research Program Symposium on Nowcasting and Very Short-Range Forecasting, WSN05, Tolouse, France, WMO, Symposium CD, Paper (Vol. 3).

Brooks, H.E., J.W. Lee, J.P. Craven, 2003: The spatial distribution of severe thunderstorm and tornado environments from global reanalysis data. – Atmos. Res. **67**, 73–94. DOI:10.1016/S0169-8095(03)00045-0.

Chou, M.-D., 1990: Parameterizations for the absorption of solar radiation by O2 and CO2 with application to climate studies. – J. Climate **3**, 209–217. DOI: 10.1175/1520-0442(1990)003<0209:PFTAOS>2.0.CO;2.

Chou, M.-D., 1992: A solar radiation model for climate studies. – J. Atmos. Sci. **49**, 762–772. DOI: 10.1175/1520-0469(1992)049<0762:ASRMFU>2.0.CO;2.

Chou, M.-D., M.J. Suarez, 1994: An efficient thermal infrared radiation parameterization for use in general circulation models. – NASA Tech Memo 104606, 85 pp. [Available from NASA Center for Aerospace Information, 800 Elkridge Landing Road, Linthicum Heights, MD 21090-2934]

Cohuet, J.B., R. Romero, V. Homar, V. Ducrocq, C. Ramis, 2011: Initiation of a severe thunderstorm over the Mediterranean Sea. – Atmos. Res. **100**, 603–620. DOI:10.1016/j.atmosres.2010.11.002.

Dotzek, N., P. Groenemeijer, B. Feuerstein, A.M. Holzer, 2009: Overview of ESSL's severe convective storms research using the European Severe Weather Database ESWD. – Atmos. Res. **93**, 575–586. DOI:10.1016/j.atmosres.2008.10.020.

Dawson, D.T., Ii, M. Xue, 2006: Numerical forecasts of the 15–16 June 2002 Southern Plains severe MCS: Impact of mesoscale data and cloud analysis. – Mon. Wea. Rev. **134**, 1607–1629. DOI:10.1175/MWR3141.1.

Ducrocq, V., D. Ricard, J.P. Lafore, F. Orain, 2002: Storm-scale numerical rainfall prediction for five precipitating events over France: On the importance of the initial humidity field. – Wea. Forecast. **17**, 1236–1256. DOI: 10.1175/1520-0434(2002)017<1236:SSNRPF>2.0.CO;2.

Gao, J., M. Xue, K. Brewster, K.K. Droegemeier, 2004: A three-dimensional variational data analysis method with recursive filter for Doppler radars. – J. Atmos. Ocean. Technol. **21**, 457–469. DOI: 10.1175/1520-0426(2004)021<0457:ATVDAM>2.0.CO;2.

García-Ortega, E., L. Fita, R. Romero, L. López, C. Ramis, J.L. Sánchez, 2007: Numerical simulation and sensitivity study of a severe hailstorm in northeast Spain. – Atmos. Res. **83**, 225–241. DOI:10.1016/j.atmosres.2005.08.004.

Grell, G.A., J. Dudhia, D.R. Stauffer, 1994: A description of the fifth-generation Penn State/NCAR mesoscale model (MM5). – NCAR Tech. Note NCAR/TN-398STR.

Horváth, Á., I. Geresdi, 2001: Severe convective storms and associated phenomena in Hungary. – Atmos. Res. **56**, 127–146. DOI:10.1016/S0169-8095(00)00094-6.

Horváth, Á., I. Geresdi, 2003: Severe storms and nowcasting in the Carpathian basin. – Atmos. Res. **67**, 319–332. DOI:10.1016/S0169-8095(03)00065-6.

Horváth, Á., I. Geresdi, P. Németh, F. Dombai, 2007: The Constitution Day storm in Budapest: Case study of the August 20, 2006 severe storm. – Idojárás **111**, 41–63.

Horvath, K., Y.L. Lin, B. Ivancan-Picek, 2008: Classification of cyclone tracks over the Apennines and the Adriatic Sea. – Mon. Wea. Rev. **136**, 2210–2227. DOI:10.1175/2007MWR2231.1

Kalnay, E., M. Kanamitsu, R. Kistler, W. Collins, D. Deaven, L. Gandin, M. Iredell, S. Saha, G. White, J. Woollen, Y. Zhu, A. Leetmaa, B. Reynolds, M. Chelliah, W. Ebisuzaki, W. Higgins, J. Janowiak, K.C. Mo, C. Ropelewski, J. Wang, R. Jenne, D. Joseph, 1996: The NCEP/NCAR 40-year reanalysis project. – Bull. Amer. Meteor. Soc. **77**, 437–472. DOI: 10.1175/1520-0477(1996)077<0437:TNYRP>2.0.CO;2.

Lin, Y.L., R.D. Farley, H.D. Orville, 1983: Bulk parameterization of the snow field in a cloud model. – J. Climate Appl. Meteor. **22**, 1065–1092. DOI: 10.1175/1520-0450(1983)022<1065:BPOTSF>2.0.CO;2.

Mastrangelo, D., K. Horvath, A. Riccio, M.M. Miglietta, 2011. Mechanisms for convection development in a long-lasting heavy precipitation event over southeastern Italy. – Atmos. Res. **100**, 586–602. DOI: 10.1016/j.atmosres.2010.10.010.

Milbrandt, J.A., M.K. Yau, 2005a: A multimoment bulk microphysics parameterization. Part I: Analysis of the role of the spectral shape parameter. – J. Atmos. Sci. **62**, 3051–3064. DOI:10.1175/JAS3534.1.

Milbrandt, J.A., M.K. Yau, 2005b: A multimoment bulk microphysics parameterization. Part II: A proposed three-moment closure and scheme description. – J. Atmos. Sci. **62**, 3065–3081. DOI:10.1175/JAS3535.1.

Miller, R.C., 1972: Notes on analysis and severe-storm forecasting procedures of the Air Force Global Weather Central. – AWS Tech. Rpt. 200 (rev), Air Weather Service, Scott AFB, IL, 109 pp.

Nuissier, O., V. Ducrocq, D. Ricard, C. Lebeaupin, S. Anquetin, 2008: A numerical study of three catastrophic precipitating events over southern France. I: Numerical framework and synoptic ingredients. – Quart. J. Roy. Meteor. Soc. **134**, 111–130. DOI:10.1002/qj.200.

Romero, R., M. Gayà, C.A. Doswell III, 2007: European climatology of severe convective storm environmental parameters: A test for significant tornado events. – Atmos. Res. **83**, 389–404. DOI:10.1016/j.atmosres.2005.06.011.

Schaefer, J.T., 1990: The critical success index as an indicator of warning skill. – Wea.Forecast. **5**, 570–575. DOI: 10.1175/1520-0434(1990)005<0570:TCSIAA>2.0.CO;2.

Seity, Y., P. Brousseau, S. Malardel, G. Hello, P. Bénard, F. Bouttier, C. Lac, V. Masson, 2011: The AROME-France convective-scale operational model. – Mon. Wea. Rev. **139**, 976–991. DOI:10.1175/2010MWR3425.1.

Showalter, A.K., 1953: A stability index for thunderstorm forecasting. – Bull. Amer. Meteor. Soc. **34**, 250–252.

Souto, M.J., C.F. Balseiro, V. Pérez-Muñuzuri, M. Xue, K. Brewster, 2003: Impact of cloud analysis on numerical weather prediction in the Galician region of Spain. – J. Appl. Meteorol. **42**, 129–140. DOI: 10.1175/1520-0450(2003)042<0129:IOCAON>2.0.CO;2.

Sun, J., 2005: Convective-scale assimilation of radar data: progress and challenges. – Quart. J. Roy. Meteor. Soc. **131**, 3439–3463. DOI:10.1256/qj.05.149.

Sun, W.Y., C.Z. Chang, 1986: Diffusion model for a convective layer. Part I: Numerical simulation of convective boundary layer. – J. Climate Appl. Meteor. **25**, 1445–1453. DOI: 10.1175/1520-0450(1986)025<1445:DMFACL>2.0.CO;2.

Strelec, N.M., A. Horváth, K. Csirmaz, 2007: Numerical simulation of severe convective phenomena over Croatian and Hungarian territory. – Atmos. Res. **83**, 121–131. DOI:10.1016/j.atmosres.2005.09.011.

Uppala, S.M., P.W. Kållberg, A.J. Simmons, U. Andrae, V.D. C. Bechtold, M. Fiorino, J.K. Gibson, J. Haseler, A. Hernandez, G.A. Kelly, X. Li, K. Onogi, S. Saarinen, N. Sokka, R.P. Allan, E. Andersson, K. Arpe, M.A. Balmaseda, A.C. M. Beljaars, L.V. D. Berg, J. Bidlot, N. Bormann, S. Caires, F. Chevallier, A. Dethof, M. Dragosavac, M. Fisher, M. Fuentes, S. Hagemann, E. Hólm, B.J. Hoskins, L. Isaksen, P.A. E.M. Janssen, R. Jenne, A.P. McNally, J.-F. Mahfouf, J.-J. Morcrette, N.A. Rayner, R.W. Saunders, P. Simon, A. Sterl, K.E. Trenberth, A. Untch, D. Vasiljevic, P. Viterbo, J. Woollen, 2005: The ERA-40 re-analysis. – Quart. J. Roy. Meteor. Soc. **131**, 2961–3012. DOI:10.1256/qj.04.176.

Xiao, Q., J. Sun, 2007: Multiple-radar data assimilation and short-range quantitative precipitation forecasting of a squall line observed during IHOP_2002. – Mon. Wea. Rev. **135**, 3381–3404. DOI:10.1175/MWR3471.1.

Xiao, Q., Y.H. Kuo, J. Sun, W.C. Lee, E. Lim, Y.R. Guo, D.M. Barker, 2005: Assimilation of Doppler Radar Observations with a Regional 3DVAR System: Impact of Doppler Velocities on Forecasts of a Heavy Rainfall Case. – J. Appl. Meteor. **44**, 768–788. DOI:10.1175/JAM2248.1.

Xue, M., K.K. Droegemeier, V. Wong, A. Shapiro, K. Brewster, 1995: ARPS version 4.0 user's guide. – Center for Analysis and Prediction of Storms, University of Oklahoma, 100 pp.

Xue, M., K.K. Droegemeier, V. Wong, 2000: The Advanced Regional Prediction System (ARPS) – A multi-scale nonhydrostatic atmospheric simulation and prediction model. Part I: Model dynamics and verification. – Meteor. Atmos. Phys. **75**, 161–193. DOI:10.1007/s007030070003.

Xue, M., K.K. Droegemeier, V. Wong, A. Shapiro, K. Brewster, F. Carr, D. Weber, Y. Liu, D. Wang, 2001: The Advanced Regional Prediction System (ARPS) – A multi-scale nonhydrostatic atmospheric simulation and prediction tool. Part II: Model physics and applications. – Meteor. Atmos. Phys. **76**, 143–166. DOI:10.1007/s007030170027.